# Analysis of mixed convection boundary layer flow of a nanofluid past a vertical plate embedded in a porous medium

A. A. Abdullah, and F. S. Ibrahim

***Abstract*—**The unsteady mixed convection flow near the stagnation point region of a heated vertical plate in a porous medium saturated with a nanofluid is studied analytically and numerically using Buongiorno's model. The model used for the nanofluid incorporates the effects of Brownian motion and thermophoresis. An appropriate similarity transforms are used and the resultant equations are solved using the fourth-fifth order Runge-Kutta method with shooting technique for different values of the parameters governing the problem. The effects of the governing parameters on fluid velocity, temperature, nanoparticle volume fraction, skin friction, Nusselt number and Sherwood number are discussed.

***Keywords*—** Nanofluid, Porous medium, Self-similar solution, Stagnation point, Unsteady mixed convection.

## I. Introduction

Stagnation-point flow generally describes the fluid motion near the stagnation region of a solid surface, which exists in the case of fixed as well as moving body in a fluid. Stagnation point flow has greater physical importance, including the prediction of skin-friction as well as heat/mass transfer near stagnation regions of bodies in high-speed flows, design of thrust bearings and radial diffusers, drag reduction, transpiration cooling and thermal oil recovery.

The flow in the neighborhood of a stagnation line has attracted many researchers during the past decades [1]-[5]. Unsteady boundary layer plays important roles in many engineering problems like start-up process and periodic fluid motion. Unsteady boundary layer has different behavior due to extra time-dependent terms, which influence the fluid motion pattern and the boundary layer separation. The problem of unsteady mixed convection flow has been investigated by several authors. Kumari et al. [6] studied the unsteady mixed convection flow of an electrically conducting fluid at the stagnation point of a two-dimensional body and an axisymmetric body in the presence of an applied magnetic field. Scshadri et al. [7] studied the unsteady mixed convection in the stagnation flow on a heated vertical plate where the unsteadiness is caused by the impulsive motion of the free stream velocity and by sudden increase in the surface temperature (heat flux). Hassanien, et al. [8] analyzed the problem of unsteady free convection flow in the stagnation-point region of a rotating sphere embedded in a porous medium. The unsteady flow and heat transfer of a viscous fluid in the stagnation region of a three-dimensional body embedded in a porous medium was investigated by [9]. Abdella and Magpantay [10] obtained approximate analytic solutions for mixed and forced convection heat transfer from an unsteady non-uniform flow past a rotating cylinder. Hassanien and Al-Arabi [11] studied the problem of thermal radiation and variable viscosity effects on unsteady mixed convection flow in the stagnation region on a vertical surface embedded in a porous medium with surface heat flux. Al-Azab [12] studied the thermophoresis effect in the problem of an unsteady mixed convection heat and mass transfer past an infinite porous plate. Fang et al. [13] investigated the boundary layers of an unsteady incompressible stagnation-point flow with mass transfer. Rosali et al. [14] discussed the effect of unsteadiness on mixed convection boundary-layer stagnation-point flow over a vertical flat surface embedded in a porous medium. The viscuss dissipation effects on unsteady natural convection flow past an infinite vertical plat with uniform heat and mass flux was discussed by [15].

During the past decade, the study of nanofluid has attracted enormous interest from researchers due to its exceptional applications to electronics, automotive, communication, computing technologies, optical devices, lasers, high-power X-rays, scientific measurement, material processing, medicine and material synthesis, where efficient heat dissipation is necessary. Nanobiotechnology is also a fast developing field of research and application in many domains, such as in medicine, pharmacy, cosmetics and agro-industry. Nanofluid are prepared by dispersing solid nanoparticles in base fluids such as water, oil or ethylene glycol. According to [16], nanofluid are produced by dispersing the nanometer-scale

This work is supported by King Abdulaziz City of Science and Technology, Saudi Arabia through its National Science, Technology and Innovation Plan (Research project No. 12-MAT2296-10).

A. A. Abdullah, Department of Mathematical Sciences, Faculty of Applied Sciences, Umm Al-Qura University, Makkah, Saudi arabia. P. O. Box 715 (phone: 00966503559660; fax: 00966125272089; e-mail: aamohammad@uqu.edu.sa).

F. S. Ibrahim, Department of Mathematics, University College, Umm Al-Qura University, Makkah, Saudi arabia. P. O. Box 715 (e-mail: fibrahim208@gmail.com).

solid particles into base liquids with low thermal conductivity such as water and ethylene glycol. Nanoparticles are usually made of metal, metal oxide, carbide, nitride and even immiscible nano-scale liquid droplets. Muthtamilselvan et al. [17] claimed that it is difficult to have a precise idea on how nanoparticles enhance the heat transfer characteristics of nanofluid.

Congedo et al. [18] compared different models of nanofluid (regarded as a single phase) to investigate the density, specific heat, viscosity and thermal conductivity and discussed the water–Al2O3 nanofluid in details by using CFD. Hamad et al. [19] introduced a one-parameter group to represent similarity reductions for the problem of magnetic field effects on free-convective nanofluid flow past a semi-infinite vertical flat plate following a nanofluid model proposed by [20]. Hady et al. [21] studied the radiation effect on viscus flow of and heat transfer over a nonlinearly stretching sheet with variable wall temperature. Also, Hady et al. [22] studied the problem of natural convection boundary layer flow past a pourus plate embedded in a porous medium saturated with a nanofluid using Buongiorno model. Further, Abu-Nada and Chamkha [23] presented the natural convection heat transfer characteristics in a differentially-heated enclosure filled with a CuO–EG–water nanofluid for different variable thermal conductivity and variable viscosity models.

The unsteady flow and heat transfer of a nanofluid over a contracting cylinder is studied by [24]. Srinivasacharya and Surender [25] studied the effects of thermal and mass stratification on natural convection boundary layer flow over a vertical plate embedded in a porous medium saturated by a nanofluid. For more information see also [26], and [27].

In this study, our main objective is to analyze the mixed convection in stagnation flow on a heated vertical surface embedded in a nanofluid-saturated porous medium. The effect of the presence of an isotropic solid matrix due to impulsive motion is considered. Moreover, we examine the combined effect of Brownian motion, thermophoresis parameters and nanoparticle fraction on boundary-layer flow and heat transfer due to nanofluid. The governing boundary layer equations are transformed to a two-point boundary value problem using similarity variables. These are numerically solved using fourth-fifth order Runge–Kutta method with shooting technique. The effects of governing parameters on fluid velocity, temperature and particle concentration are discussed and shown graphically and in tables as well.

## II. Mathematical Formulation

Let us consider a semi-infinite vertical plate embedded in a saturated porous medium with temperature $T_w$ and nanoparticle volume fraction $\varphi_w$. The ambient temperature and nanoparticle volume fraction are $T_\infty$ and $\varphi_\infty$ respectively. At $t=0$ the ambient fluid is impulsively moved with a velocity $U_e$ and at the same time the surface temperature is raised suddenly. The assisting flow occurs if the upper half of the plate is heated while the lower half of the plate is cooled. In this case, with considering the buoyancy force the flow near the heated plate tends to move upward and the flow near the cooled plate tends to move downward, therefore this behavior acts to assist the main flow field. The opposing flow occurs if the upper part of the plate is cooled while the lower part of the plate is heated. The physical flow model and coordinate system is shown in Fig. 1.

Under above assumptions along with Boussinesq and boundary layer approximations, the governing equations of the conservation of mass, momentum, energy and nanoparticles volume fraction can be expressed as:

$$\nabla.\vec{v}=0\ , \tag{1}$$

$$\rho_f\left(\frac{\partial\vec{v}}{\partial t}+\vec{v}.\nabla\vec{v}\right)=-\nabla P+\mu\nabla^2\vec{v}-\frac{\mu\varepsilon}{K}\vec{v}-\frac{\Gamma\varepsilon^2}{K^{1/2}}\rho_f|\vec{v}|\vec{v} + \left[\rho_f(1-\varphi_\infty)\beta_T(T-T_\infty)-(\rho_p-\rho_f)(\varphi-\varphi_\infty)\right]\vec{g} \tag{2}$$

$$(\rho c)_m\frac{\partial T}{\partial t}+(\rho c)_f\vec{v}.\nabla T=k_m\nabla^2T + \varepsilon(\rho c)_p\left[D_B\nabla\varphi.\nabla T+\frac{D_T}{T_\infty}\nabla T.\nabla T\right] \tag{3}$$

$$\frac{\partial\varphi}{\partial t}+\vec{v}.\nabla\varphi=D_B\nabla^2\varphi+\frac{D_T}{T_\infty}\nabla^2T \tag{4}$$

where $\vec{v}=(u,v)$ is the velocity, $T$ is the temperature , $\varphi$ is the nanoparticle concentration, $\vec{g}$ is the acceleration due to gravity, $\rho_f$ and $\rho_p$ are the densities of the base fluid and nanoparticles respectively, $K$ is the permeability of the porous medium, $\varepsilon$ is the porosity, $\Gamma$ is the empirical constant in the second order resistance, $\mu, k_m$ and $\beta_T$ are the viscosity, thermal conductivity and volumetric thermal expansion coefficients of the nanofluid, $(\rho c)_f$ is the heat capacity of the fluid and $(\rho c)_p$ is the effective heat capacity of the nanoparticle material, $(\rho c)_m$ is the effective heat capacity and $D_B$ and $D_T$ are the Brownian diffusion coefficient and the thermophoretic diffusion coefficient respectively. The proposed initial conditions are

$$u(t,x,y)=v(t,x,y)=0,\quad T(t,x,y)=T_\infty,\quad \varphi(t,x,y)=\varphi_\infty\quad for\ t<0. \tag{5}$$

The proposed boundary conditions for $t\geq 0$ are

$$u(t,x,0)=v(t,x,0)=0,\quad u(t,x,\infty)=U_e(t,x)=ax/(1-ct),\quad T(t,x,0)=T_w(t,x)=T_\infty+bx/(1-ct)^2,\quad T(t,x,\infty)=T_\infty,\quad \varphi(t,x,0)=\varphi_w(t,x)=\varphi_\infty+bx/(1-ct)^2,\quad \varphi(t,x,\infty)=\varphi_\infty \tag{6}$$

where a and c are constants and both have dimension time−1 (with a > 0, c ≥ 0, and ct < 1), and b is a constant and has

dimension temperature/length, with b > 0 and b < 0 correspond to the assisting and opposing flows, respectively, and *b = 0* corresponds to forced convection limit (absence of buoyancy force).

We now make the standard boundary layer approximation, based on the scale analysis. Thus the governing equations become

$$\frac{\partial u}{\partial x}+\frac{\partial v}{\partial y}=0 \tag{7}$$

$$\rho_f\left[\frac{\partial u}{\partial t}+u\frac{\partial u}{\partial x}+v\frac{\partial u}{\partial y}\right]=-\frac{\partial p}{\partial x}+\mu\frac{\partial^2 u}{\partial y^2}-\frac{\mu\varepsilon}{K}u-\frac{\Gamma\varepsilon^2}{K^{1/2}}\rho_f u^2+[(1-\varphi_\infty)\beta_T\rho_f(T-T_\infty)-(\rho_p-\rho_f)(\varphi-\varphi_\infty)]g \tag{8}$$

$$\sigma\frac{\partial T}{\partial t}+u\frac{\partial T}{\partial x}+v\frac{\partial T}{\partial y}=\alpha_m\frac{\partial^2 T}{\partial y^2}+\tau\left[D_B\frac{\partial T}{\partial y}\frac{\partial\varphi}{\partial y}+\frac{D_T}{T_\infty}\left(\frac{\partial T}{\partial y}\right)^2\right] \tag{9}$$

$$\frac{\partial\varphi}{\partial t}+\frac{1}{\varepsilon}(u\frac{\partial\phi}{\partial x}+v\frac{\partial\varphi}{\partial y})=D_B\frac{\partial^2\varphi}{\partial y^2}+\frac{D_T}{T_\infty}\left(\frac{\partial^2 T}{\partial y^2}\right) \tag{10}$$

where $x$ and $y$ are the coordinates along and normal to the surface respectively, $\alpha_m=k_m/(\rho c)_f$ is the thermal diffusivity, $\tau=(\rho c)_p/(\rho c)_f$ is the ratio of the effective heat capacity of the nanoparticle material to the heat capacity of the fluid and $\sigma=(\rho c)_m/(\rho c)_f$ is the ratio of the effective heat capacity of the porous medium to the heat capacity of the fluid. Outside the boundary layer, (8) gives

$$-\frac{\partial p}{\partial x}=\rho_f\left(\frac{\partial U_e}{\partial t}+U_e\frac{\partial U_e}{\partial x}\right)+\frac{\mu\varepsilon}{K}U_e+\frac{\Gamma\varepsilon^2}{K^{1/2}}\rho_f U_e^2 \tag{11}$$

from which we can eliminate the pressure p from the momentum equation. Now let us introduce the stream function $\psi$ such that

$$u=\frac{\partial\psi}{\partial y},\quad v=-\frac{\partial\psi}{\partial x} \tag{12}$$

then the continuity equation, (7), is satisfied identically and the remaining governing equations (8-10) become

$$\frac{\partial^2\psi}{\partial t\partial y}+\left(\frac{\partial\psi}{\partial y}\frac{\partial^2\psi}{\partial x\partial y}-\frac{\partial\psi}{\partial x}\frac{\partial^2\psi}{\partial y^2}\right)=\frac{\partial U_e}{\partial t}+U_e\frac{\partial U_e}{\partial x}+\upsilon\frac{\partial^3\psi}{\partial y^3}+\frac{\nu}{K}(U_e-u)+\frac{\Gamma\varepsilon}{K^{1/2}}(U_e^2-u^2)+[(1-\varphi_\infty)\beta_T(T-T_\infty)-(\rho_p-\rho_f)(\varphi-\varphi_\infty)/\rho_f]g \tag{13}$$

$$\sigma\frac{\partial T}{\partial t}+\frac{\partial\psi}{\partial y}\frac{\partial T}{\partial x}-\frac{\partial\psi}{\partial x}\frac{\partial T}{\partial y}=\alpha_m\frac{\partial^2 T}{\partial y^2}+\tau\left[D_B\frac{\partial T}{\partial y}\frac{\partial\varphi}{\partial y}+\frac{D_T}{T_\infty}\left(\frac{\partial T}{\partial y}\right)^2\right] \tag{14}$$

$$\frac{\partial\varphi}{\partial t}+\frac{1}{\varepsilon}(\frac{\partial\psi}{\partial y}\frac{\partial\phi}{\partial x}-\frac{\partial\psi}{\partial x}\frac{\partial\varphi}{\partial y})=D_B\frac{\partial^2\varphi}{\partial y^2}+\frac{D_T}{T_\infty}\left(\frac{\partial^2 T}{\partial y^2}\right) \tag{15}$$

The particular forms of $U_e(t,x)$, $T_w(t,x)$ and $\varphi_w(t,x)$ in the boundary conditions (6) have been chosen in order to obtain a new similarity transformation, which transforms the governing partial differential equations (13-15) into a set of coupled ordinary differential equations. The mathematical analysis of the problem is simplified by introducing the following similarity transforms as suggested by Kumari et al. [14]:

$$\eta=\sqrt{\frac{a}{\upsilon(1-ct)}}y,\quad \psi=\sqrt{\frac{a\upsilon}{1-ct}}\,x\,f(\eta),\quad \theta(\eta)=\frac{T-T_\infty}{T_w-T_\infty},\quad \phi(\eta)=\frac{\varphi-\varphi_\infty}{\varphi_w-\varphi_\infty} \tag{16}$$

Using the similarity transforms, the governing equations (13-15) transformed to the following ordinary differential equations

$$f'''+1+A(1-f'-\frac{1}{2}\eta f'')-f'^2+f\,f''+\lambda(\theta-N_r\,\phi)+\gamma(1-f')+\Delta(1-f'^2)=0, \tag{17}$$

$$\frac{1}{\Pr}\theta''-A(2\theta+\frac{1}{2}\eta\theta')-f'\theta+f\,\theta'+N_b\,\theta'\phi'+N_t\,\theta'^2=0, \tag{18}$$

$$\frac{1}{Le}\phi''-A(2\phi+\frac{1}{2}\eta\phi')-f'\phi+f\,\phi'+\frac{1}{Le}\frac{N_t}{N_b}\theta''=0, \tag{19}$$

and the boundary conditions (5) and (6) become

$$f'(\eta)=0,\quad f(\eta)=0,\quad \theta(\eta)=0,\quad \phi(\eta)=0,\quad for\quad t<0, \tag{20}$$

$$f(0)=0,\quad f'(0)=0,\quad \theta(0)=1,\quad \phi(0)=1,$$
$$f'(\infty)=1,\quad \theta(\infty)=0,\quad \phi(\infty)=0,\qquad for\quad t\geq 0 \tag{21}$$

where

$$A=\frac{c}{a},\quad \Pr=\frac{\nu}{\alpha},\quad Le=\frac{\nu}{D_B},\quad \lambda=\frac{Gr_x}{\mathrm{Re}_x^2},$$

$$\gamma=\frac{1}{Da_x\,\mathrm{Re}_x},\quad \Delta==\frac{\Gamma}{Da_x^{1/2}},\ N_b=\frac{\tau}{\nu}D_B(\varphi_w-\varphi_\infty),$$

$$N_t=\frac{\tau}{\nu}\left(\frac{D_T}{T_\infty}\right)(T_w-T_\infty),\quad N_r=\frac{(\rho_p-\rho_f)(\varphi_w-\varphi_\infty)}{\beta\rho_f(1-\varphi_\infty)(T_w-T_\infty)}$$

Here $f'$, $\theta$ and $\phi$ are the dimensionless velocity, temperature and nanoparticles volume fraction, respectively. The prime

denotes differentiation with respect to the similarity variable $\eta$. Also

$$Gr_x = \frac{g\beta_T(1-\varphi_\infty)(T_w - T_\infty)x^3}{\nu^2},\ \mathrm{Re}_x = \frac{U_e\, x}{\nu},\ Da_x = K/x^2$$

are Grashof, Reynolds and Darcy numbers, respectively. A, $\lambda$, $Pr$, $Le$, $N_t$, $N_b$, $N_r$, $\gamma$ and $\Delta$ denotes the unsteadiness parameter, mixed convection parameter, Prandtl number, Lewis number, thermophoresis parameter, Brownian motion parameter, nanofluid buoyancy ratio, first resistant parameter and second resistant parameter, respectively.

The important physical quantities of interest in this problem are the skin friction coefficient (wall shear stress), $C_f$, local Nusselt number, $Nu_x$, and local Sherwood number, $Sh_x$, which are defined by

$$C_f = \frac{\mu}{\rho U_\infty^2}\left(\frac{\partial u}{\partial y}\right)_{y=0},\quad Nu_x = \frac{x}{(T_w - T_\infty)}\left(\frac{\partial \theta}{\partial y}\right)_{y=0},$$
$$Sh_x = \frac{x}{(\varphi_w - \varphi_\infty)}\left(\frac{\partial \varphi}{\partial y}\right)_{y=0}. \qquad (22)$$

Using (16) we obtain

$$C_f = \mathrm{Re}_x^{1/2}\, f''(0),\quad Nu_x = -\mathrm{Re}_x^{-1/2}\,\theta'(0),$$
$$Sh_x = -\mathrm{Re}_x^{-1/2}\,\phi'(0). \qquad (23)$$

## III. Results and Discussion

The resulting differential system (17)–(19) subjected to the boundary conditions (20) and (21) are solved numerically using fourth-fifth order Runge–Kutta method (RK45) with a shooting technique.

To facilitate convergence for all values of parameters, the asymptotic boundary conditions given by (21) were replaced by using a value of 6 for the similarity variable $\eta_{\max}$ as follows.

$$\eta_{\max} = 6,\ f'(6) = 1,\ \theta(6) = 0,\ \gamma(6) = 0,\ \phi(6) = 0.$$

The choice of $\eta_{\max} = 6$ ensured that all numerical solutions approached the asymptotic values correctly. This is an important point that is often overlooked in publications on boundary layer flows. Many published results on boundary layer flows are erroneous because the graphs for the velocity and temperature distributions in the boundary layers do not approach the correct values asymptotically. All the errors were the consequence of using smaller values of $\eta$ to represent the boundary condition as $\eta \to \infty$.

In order to test the accuracy of our method, we have compared our results for the steady-state case ($A = 0$) for the skin friction and heat transfer rate for prescribed surface temperature with those of Ramachandran et al. [l]. The results are found to be in excellent agreement as shown in table I.

The values of the governing parameters are chosen arbitrary. However, the numerical results are presented for some representative values of these governing parameters. In order to see the physical insight, the numerical values of velocity, $f'(\eta)$, temperature, $\theta(\eta)$, and nanoparticle volume fraction, $\phi(\eta)$, with the boundary layer have been computed for different parameters as unsteadiness parameter, $A$, mixed convection parameter, $\lambda$, nanofluid buoyancy ratio parameter, $N_r$, thermophoresis parameter, $N_t$, Brownian motion parameter, $N_b$, first resistant parameter, $\gamma$, second resistant parameter, $\Delta$, Prandtl number, $Pr$, and Lewis number, $Le$.

Table II lists results of the gradients of velocity, temperature and volume fraction functions, which are proportional to the skin friction factor, Nusselt number and Sherwood number, respectively. From this table, we notice that as $N_r$ increases, the friction factor, the heat transfer rate (Nusselt number) and mass transfer rate (Sherwood number) decrease. As $N_t$ and $N_b$ increase, the friction factor and surface mass transfer rates increase whereas the surface heat transfer rate decreases.

The effects of the first and second resistances of the porous medium on the gradients of velocity, temperature and volume fraction functions are illustrated in Table III. From this table we conclude that both the first and second resistances enhance the wall shear stress and the mass transfer rate and reduce the heat transfer rate.

The numerical solutions for the dimensionless velocity, temperature and nanoparticle volume fraction are obtained and presented in Figs. 2–10. The effects of all parameters governing the problem are discussed.

The variation of the non-dimensional velocity, temperature and nanoparticle concentration for

$$N_t = 0.5, N_b = 0.5, N_r = 1.0, \lambda = 1.0, \mathrm{Pr} = 10, Le = 10,$$
$$\gamma = 0.5,\ \Delta = 0.5$$

with unsteadiness parameter $A$ is illustrated in Fig. 2. It can be observed from Fig. 2(a) that for velocity distribution, there is a special point ( $\eta \approx 1.4$ ) called 'crossing over point' and the velocity profiles have conflicting behavior before and after that point. The value of the velocity profile for fixed η increases before that point and slightly decreases after that. Thus, due to the increase of unsteadiness parameter, $A$, the velocity initially enhances but ultimately it increases the thickness of momentum boundary layer. On the other hand the temperature and nanoparticle volume fraction profiles of Figs. 2 (b, c), show that the unsteadiness controls the heat and mass transfer. The control of heat and mass transfer is of great practical significance. As $A$ increases, the temperature and nanoparticle volume fraction at a point decrease because the thermal boundary-layer thickness rapidly decreases due to increase of unsteadiness.

The effect of mixed convection parameter $\lambda$ on the non-dimensional velocity, temperature and nanoparticle volume fraction is illustrated in Fig. 3. From this figure, it is observed

that the velocity increases as $\lambda$ increases, however both the temperature and nanoparticle fraction decrease with increasing $\lambda$. The velocity profile decreases and both the temperature and nanoparticle volume fraction increase as nanofluid buoyancy ratio parameter $N_r$ increases as shown in in Fig. 4.

Figure 5 presents the effect of thermophoresis $N_t$ on the velocity, temperature and volume fraction distributions. It is observed that the momentum boundary-layer thickness increases with an increase of $N_t$. As the parameter $N_t$ increases, the thermal and nanoparticle volume fraction boundary-layer thickness increase for specific conditions.

Furthermore, increasing the value of the Brownian motion $N_b$ causes a thickening of momentum and thermal boundary layers and thinning of the nanoparticle volume fraction boundary layer as shown in Fig. 6. Physically, it is true due to the fact that large values of the Brownian motion parameter impact a large extent of the fluid. It results in the thickening of the momentum and thermal boundary layers. Hence, the present analysis shows that the flow field is appreciably influenced by the Brownian motion $N_b$

The effect of both first resistant parameter $\gamma$ and second resistant parameter $\Delta$ is shown in Fig. 7 and Fig. 8, respectively. From these figures, it is observed that both $\gamma$ and $\Delta$ have the same behavior. The velocity profile increases but the temperature profile and volume fraction profile decrease as both $\gamma$ and $\Delta$ increase.

The effect of Prandtl number *Pr* is illustrated in Fig. 9. From this figure, it is observed that as *Pr* increases the velocity and temperature profiles decrease. On the other hand, for the volume fraction profiles there is a crossing over point at ( $\eta \approx 0.5$ ) where the volume fraction profile decreases before that point and slightly increases after that.

It is clear from Fig. 10 that an increase in the Lewis number Le results in an increase in the velocity and a decrease in the volume fraction within the boundary layer. In the temperature profile there is a crossing over point at ( $\eta \approx 0.8$ ) where the temperature profiles have completely conflicting behavior before and after that point. The value of the temperature profile for fixed $\eta$ decreases before that point and slightly increases after it. The present analysis shows that the flow field is appreciably influenced by the Lewis number *Le*.

## ACKNOWLEDGMENT

The authors are grateful for the financial support of this project from King Abdulaziz City of Science and Technology, Saudi Arabia through its National Science, Technology and Innovation Plan (Research project No. 12-MAT2296-10).

## REFERENCES

[1] N. Ramachandran, T. Chen and B. Armaly, "Mixed convection in the stagnation flows adjacent to vertical surface," *J. Heat Transf.* vol. 110, pp. 173–177, 1988.

[2] A. Ishak, R. Nazar and I. Pop, "Mixed convection flow of a viscoelastic fluid near the orthogonal stagnation-point on a vertical surface," *Int.* J. Heat Mass Transf. vol. 51, pp. 1150–1155, 2008.

[3] D. Li, F. Labropulu and I. Pop, "Dual solutions in mixed convection flow near a stagnation point on a vertical surface in a porous medium," *Int. J. Therm. Sci.* vol. 50, pp. 1698–1705, 2011.

[4] O. Makinde, "Heat and mass transfer by MHD mixed convection stagnation point flow toward a vertical plate embedded in a highly porous medium with radiation and internal heat generation," *Meccanica* vol. 47, pp. 1173–1184, 2012.

[5] F. Mabood and W. Khan, "Approximate analytic solutions for influence of heat transfer on MHD stagnation point flow in porous medium," *Comput. Fluids* vol. 100, pp. 72–78, 2014.

[6] M. Kumari, H. Takhar and G. Nath, "Unsteady mixed convection flow at the stagnation point," *Int. J. Eng. Sci.* vol. 30, pp. 1789-1800, 1992.

[7] R. Scshadri, N. Srccshylan and G. Nath, "Unsteady mixed convection flow in the stagnation region of a heated vertical plate due to impulsive motion," *Int. J. Heat Mass Transf.* vol. 45, pp. 1345-1352, 2002.

[8] I. Hassanien, F. Ibrahim and Gh. Omer, "Unsteady free convection flow in the stagnation-point region of a rotating sphere embedded in a porous medium," *Mech. Mech. Eng.* vol. 7, pp. 89-98, 2004.

[9] I. Hassanien, F. Ibrahim and Gh. Omer, "Unsteady flow and heat transfer of a viscous fluid in the stagnation region of a three-dimensional body embedded in a porous medium," *J. Porous Media* vol. 9, pp. 357-372, 2006.

[10] K. Abdella and F. Magpantay, "Approximate analytic solutions for mixed and forced convection heat transfer from an unsteady non-uniform flow past a rotating cylinder," *Wseas Trans. Heat Mass Transf.* vol. 2, pp. 6-16, 2007.

[11] I. Hassanien and T. Al-Arabi, "Thermal radiation and variable viscosity effects on unsteady mixed convection flow in the stagnation region on a vertical surface embedded in a porous medium with surface heat flux," *Far East J. Math. Sci.* vol. 29, pp. 187–207, 2008.

[12] T. Al-Azab, "Unsteady mixed convection heat and mass transfer past an infinite porous plate with thermophoresis effect," *Wseas Trans. Heat Mass Transf.* vol. 4, pp. 23-33, 2009.

[13] T. Fang, C. Lee and J. Zhang, "The boundary layers of an unsteady incompressible stagnation-point flow with mass transfer," *Int. J. Nonlinear Mech.* vol. 46, pp. 942–948, 2011.

[14] H. Rosali, A. Ishak, R. Nazar, J. Merkin and I. Pop, "The effect of unsteadiness on mixed convection boundary-layer stagnation-point flow over a vertical flat surface embedded in a porous medium," *Int. J. Heat Mass Transf.* vol. 77, pp. 147–156, 2014.

[15] P. Loganathan and C. Sivapoornapriya, "Viscous dissipation effects on unsteady natural convective flow past an infinite vertical plate with uniform heat and mass flux," *Wseas Trans. Heat Mass Transf.* vol. 9, pp. 63-73, 2014.

[16] N. Yacob, A. Ishak and I. Pop, "Falkner–Skan problem for a static or moving wedge in nanofluids," *Int. J. Therm. Sci.* vol. 50, pp. 133–139, 2011.

[17] M. Muthtamilselvan, P. Kandaswamy and J. Lee, "Heat transfer enhancement of copper–water nanofluids in a lid-driven enclosure," *Commun. Nonlinear Sci. Numer. Simul.* vol. 15, pp. 1501–1510, 2010.

[18] P. Congedo, S. Collura and P. Congedo, "Modelling and analysis of natural convection heat transfer in nanofluids," *Proc. ASME Summer Heat Transf. Conf.* vol. 3, pp. 569–579, 2009.

[19] M.Hamad, I. Pop, and A. Ismail, "Magnetic field effects on free convection flow of a nanofluid past a semi-infinite vertical flat plate," *Nonlinear Anal-Real* vol. 12, pp. 1338–1346, 2011.

[20] J. Buongiorno, "Convective transport in nanofluids," *ASME J. Heat Transf.* vol. 128, pp. 240–250, 2006.

[21] H. Hady, F. Ibrahim, S. Abdel-Gaid and M. Eid, "Radiation effect on viscous flow of a nanofluid and heat transfer over a nonlinearly stretching sheet," *Nanoscale Res. Lett.* vol. 7, pp. 229–241, 2012.

[22] F. Hady, F. Ibrahim, H. El-Hawary, and A. Abdelhady, "Effect of suction/injection on natural convective boundary-layer flow of a nanofluid past a vertical porous plate through a porous medium," *J. Mod. Meth. Numer. Math.* vol. 3, pp. 53–63, 2012.

[23] E. Abu-Nada and A. Chamkha, "Effect of nanofluid variable properties on natural convection in enclosures filled with a CuO–EG–water nanofluid," *Int. J. Therm. Sci.* vol. 49, pp. 2339–2352, 2010.

[24] K. Zaimi, A. Ishak and I. Pop, "Unsteady flow due to a contracting cylinder in a nanofluid using Buongiorno's model," *Int. J. Heat Mass Transf.* vol. 68, pp. 509-513, 2014.

[25] D. Srinivasacharya and O. Surender, "Non-similar solution for natural convective boundary layer flow of a nanofluid past a vertical plate embedded in a doubly stratified porous medium," *J Heat Mass Transf.* vol. 71, pp. 431-438, 2014.

[26] S. Das, S. Choi, W. Yu and T. Pradeep, *Nanofluids: Science and Technology*. New Jersey: Wiley, 2008.

[27] S. Kakac and A. Pramuanjaroenkij, "Review of convective heat transfer enhancement with nanofluids," *Int J Heat Mass Transf.* vol. 52, pp. 3187–3196, 2009.

**Abdullah A. Abdullah** (Makkah, Saudi Arabia 12/2/1960).
B.Sc. in mathematics, Umm Al-Qura University, Makkah, Saudi Arabia 1981. M.Sc. in applied mathematics (fluid mechanics), Glasgow University, Glasgow, Scotland, U.K. 1987. Ph.D. in applied mathematics (fluid mechanics), Glasgow University, Glasgow, Scotland, U.K. 1990.

He worked as a PROGRAMMER in the computer center, Umm Al-Qura University 1982-1983 then he joined Umm al-Qura University as a TEACHING ASSISTANCE in the department of Mathematical Sciences, Faculty of Applied Science 1984. He became ASSISTANT PROFESSOR in the department of Mathematical sciences, Faculty of Applied ciences, Umm Al-Qura University in 1990, ASSOCIATE PROFESSOR in 1997 and a PROFESSOR in 2002. Beside his academic work he worked as a HEAD OF THE DEPARTMENT OF COMPUTER AND INFORMATION in Hajj research center, Umm Al-Qura University during the period 1993-1997, as a VICE DEAN OF ADMISSION AND REGISTRATION, Umm Al-Qura University during the period 1997-2003, a DEAN OF ADMISSION AND REGISTRATION, Umm Al-Qura University during the period 2003-2010, a DEAN OF THE DEANSHIP OF PREPARATORY YEAR of Umm Al-Qura University during the period 2010- 2013. He is a consultant of "Fakieh research and development center " in Makkah, Saudi Arabia 2001-till now. His recent publications are:

- H. Banjer and Abdullah, Thermal instability in superposed porous and fluid layers in the presence of a magnetic field using Brinkman model," *J. Porous Media*. vol. 15, no. 1, pp. 1-10, 2012.
- A. Abdullah and Z. Rashed, "Benard-Marangoni convection in a porous layer permeated by a non-linear magnetic fluid," *Int. J. of Appl. Math. And Mech*. vol. 8 no. 12, pp. 13-41, 2012.
- A. Abdullah and S. Alkazmi, "Thermohaline convection in a porous medium in the presence of magnetic field and rotation," *Develop. appl. oceanic eng.* vol. 3, pp. 32-38, 2014.

His current interests is in the area of thermal instability of fluids and some applications regarding solar energy.

He is a member of the Saudi Arabian society of Mathematical Sciences and a reviewer of the International Journal of Numerical Methods for Heat & Fluid Flow.

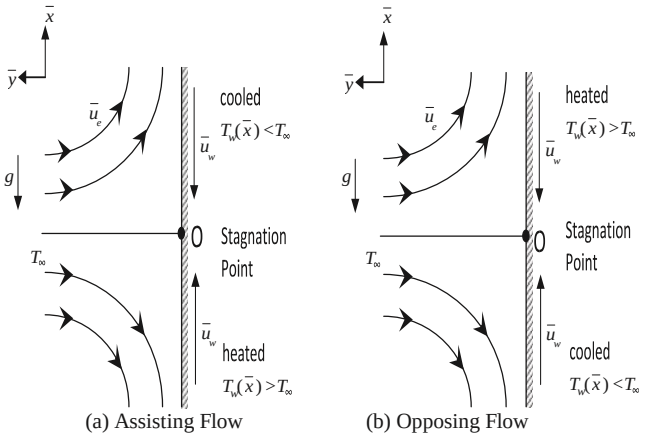


(a) Assisting Flow (b) Opposing Flow

**Fig. 1** Physical model and coordinate system

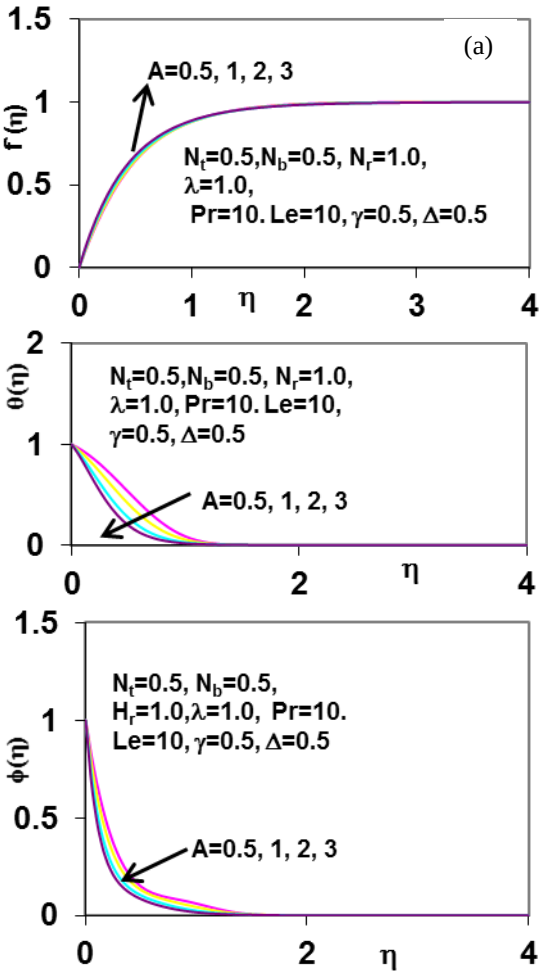


**Fig. 2** Effects of unsteadiness parameter $A$ on (a) velocity, (b) Temperature and (c) Nanoparticle volume fraction profiles.

**Fig**

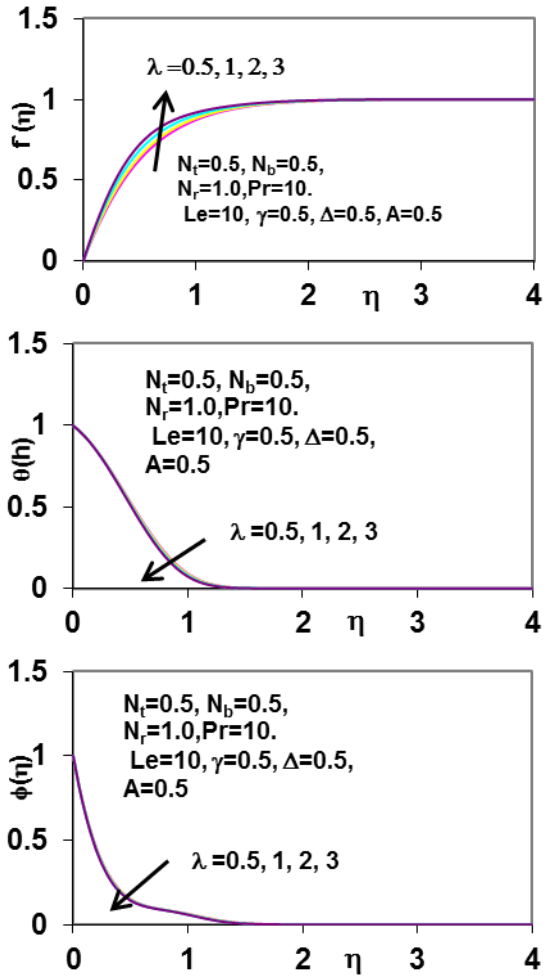


**Fig. 3** Effects of mixed convection parameter $\lambda$ on (a) velocity, (b) Temperature and (c) Nanoparticle volume fraction profiles.

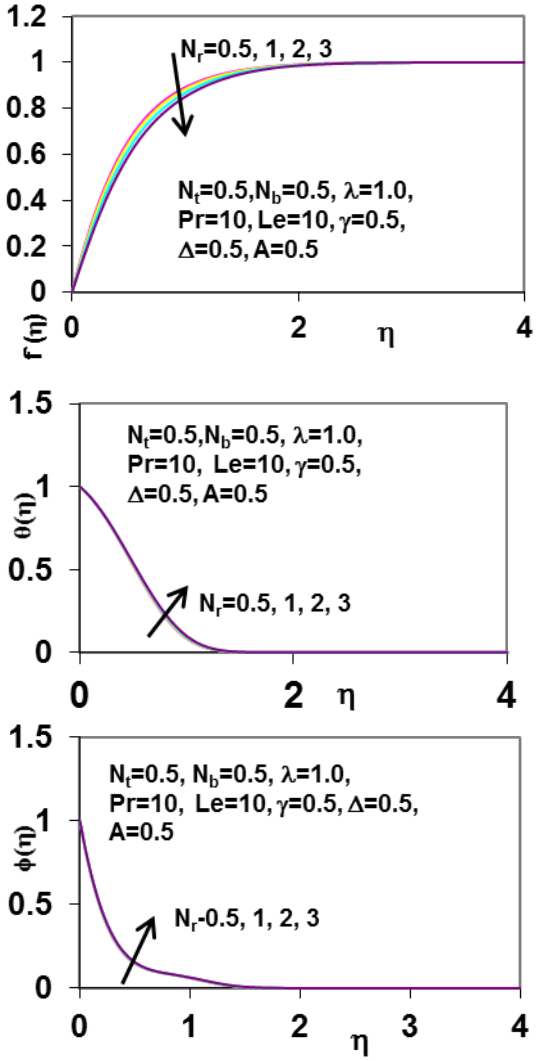


**Fig. 4** Effects of nanofluid buoyancy ratio parameter $N_r$ on (a) velocity, (b) Temperature and (c) Nanoparticle volume fraction.

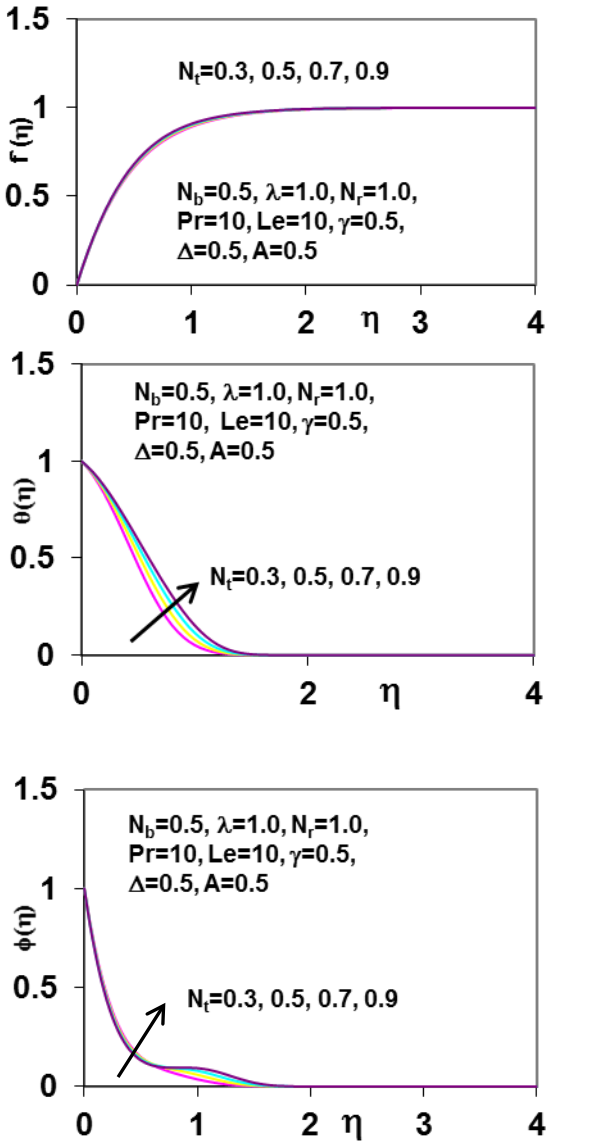


**Fig. 5** Effects of thermophoresis parameter $N_t$ on (a) velocity, (b) Temperature and (c) Nanoparticle volume fraction profiles.

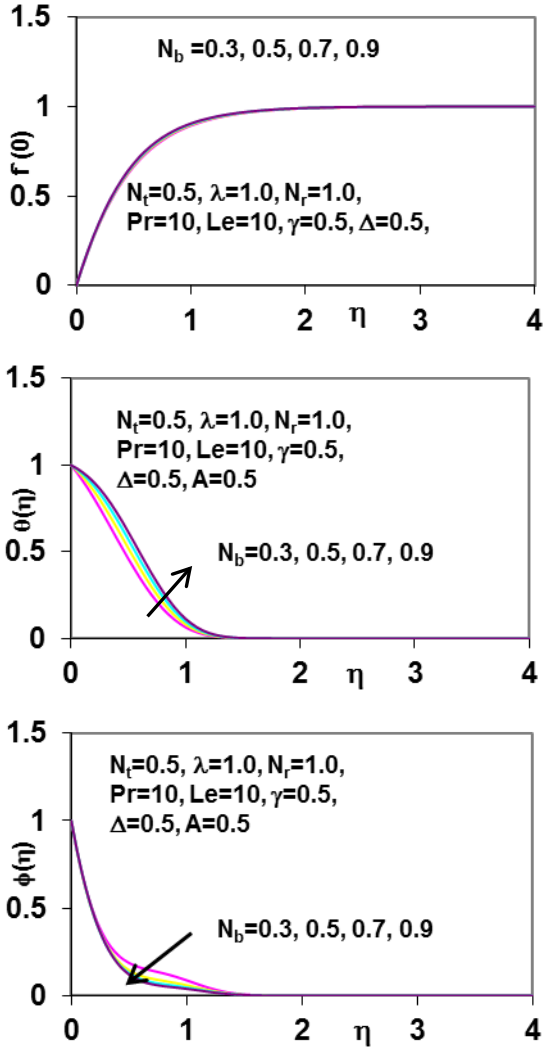


**Fig. 6** Effects of Brownian motion parameter $N_b$ on (a) velocity, (b) Temperature and (c) Nanoparticle volume fraction profiles.

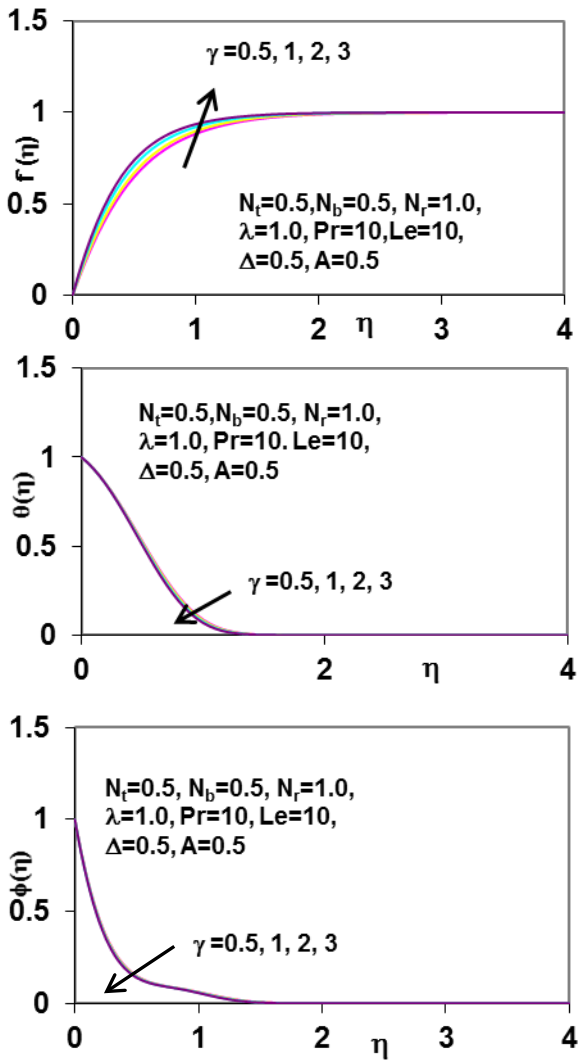


**Fig. 7** Effects of first resistant parameter $\gamma$ on (a) velocity, (b) Temperature and (c) Nanoparticle volume fraction profiles.

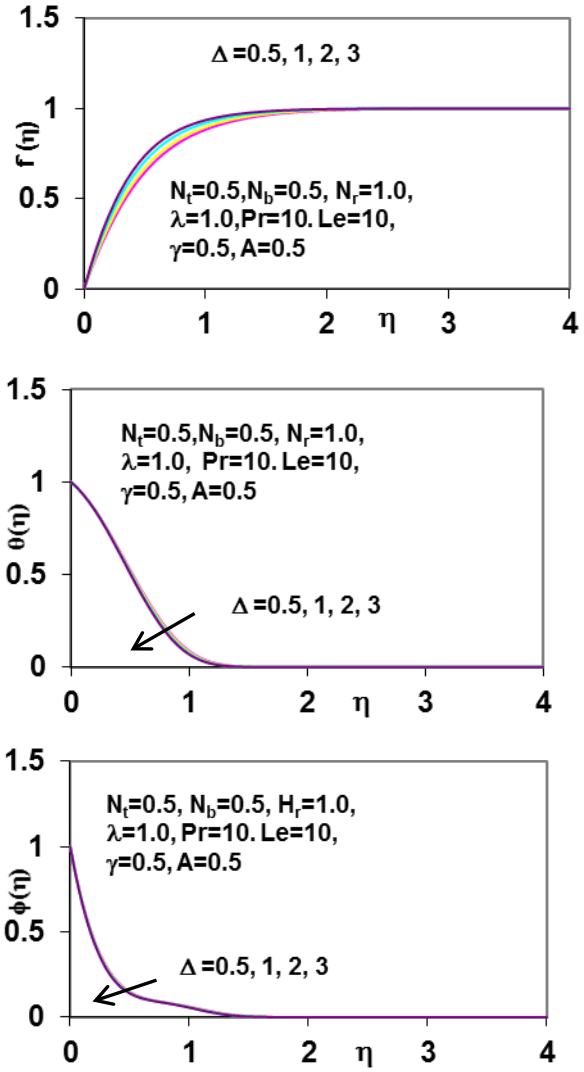


**Fig. 8** Effects of second resistant parameter $\Delta$ on (a) velocity, (b) Temperature and (c) Nanoparticle volume fraction profiles.

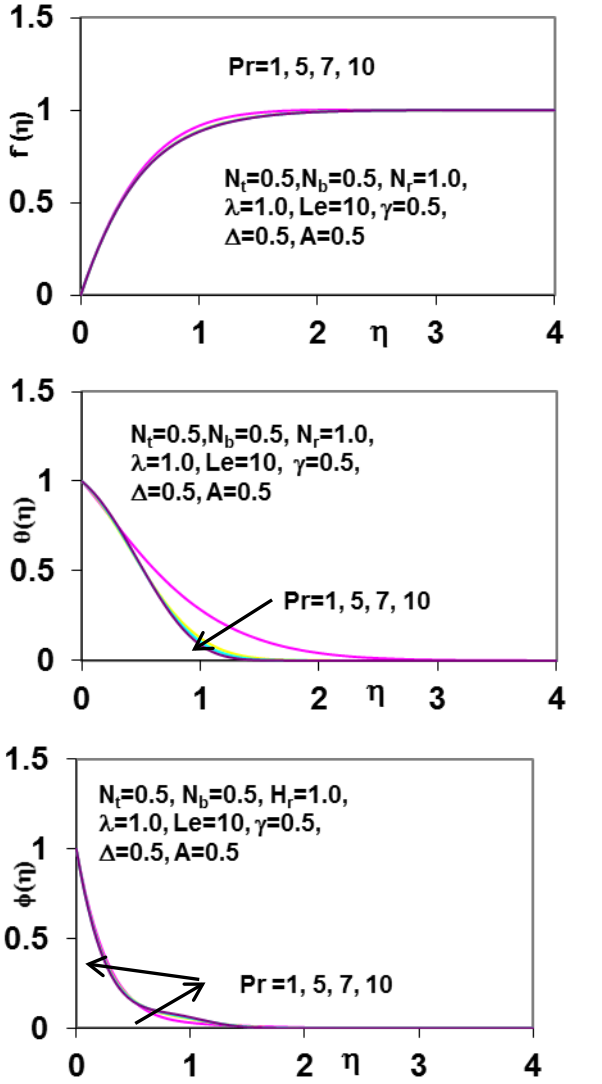


**Fig. 9** Effects of Prandtl number *Pr* on (a) velocity, (b) Temperature and (c) Nanoparticle volume fraction profiles.

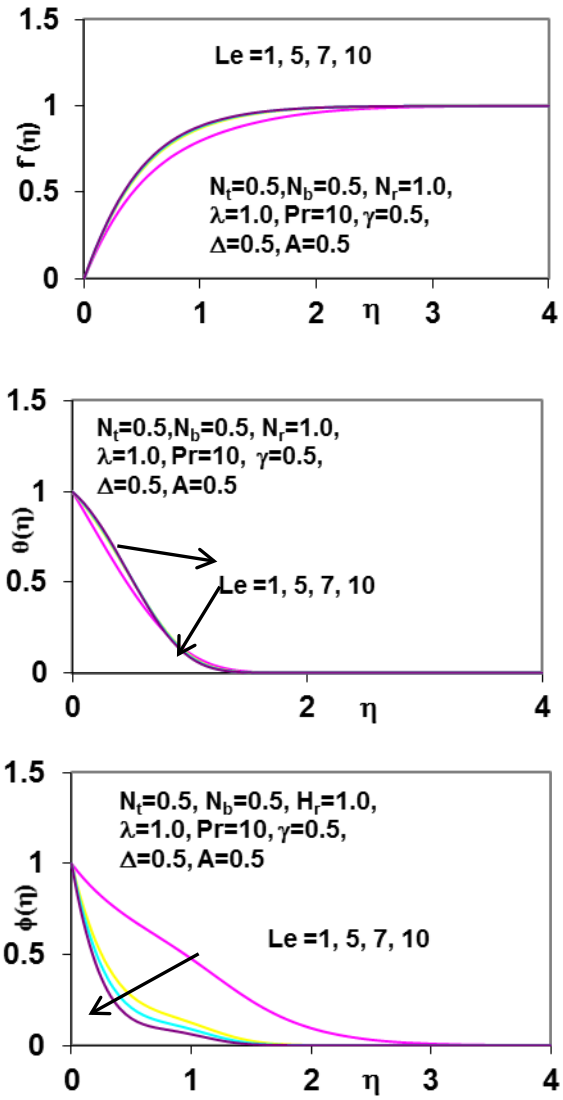


**Fig. 10** Effects of Lewis number $Le$ on (a) velocity, (b) Temperature and (c) Nanoparticle volume fraction profiles.

**Caption of figures**

**Fig. 1** Physical model

**Fig. 2** Effects of unsteadiness parameter $A$ on (a) velocity, (b) Temperature and (c) Nanoparticle volume fraction profiles

**Fig. 3** Effects of mixed convection parameter $\lambda$ on (a) velocity, (b) Temperature and (c) Nanoparticle volume fraction profiles

**Fig. 4** Effects of nanofluid buoyancy ratio parameter $N_r$ on (a) velocity, (b) Temperature and (c) Nanoparticle volume fraction profiles

**Fig. 5** Effects of thermophoresis parameter $N_t$ on (a) velocity, (b) Temperature and (c) Nanoparticle volume fraction profiles

**Fig. 6** Effects of Brownian motion parameter $N_b$ on (a) velocity, (b) Temperature and (c) Nanoparticle volume fraction profiles

**Fig. 7** Effects of first resistant parameter $\gamma$ on (a) velocity, (b) Temperature and (c) Nanoparticle volume fraction profiles

**Fig. 8** Effects of second resistant parameter $\Delta$ on (a) velocity, (b) Temperature and (c) Nanoparticle volume fraction profiles

**Fig. 9** Effects of Prandtl number Pr on (a) velocity, (b) Temperature and (c) Nanoparticle volume fraction profiles

**Fig. 10** Effects of Lewis number $Le$ on (a) velocity, (b) Temperature and (c) Nanoparticle volume fraction profiles

**Table I** Comparison of skin fraction $f''(0)$ and heat transfer rate $-\theta'(0)$ for steady-state flow ( $A = 0$ ) when assisting ( $\lambda = 1$ ) and opposing flow ( $\lambda = -1$ ) flow with those of Ramachandran et al. [l].

| $P_r$ | $\lambda$ = 1 | | | | $\lambda$ = -1 | | | |
|---|---|---|---|---|---|---|---|---|
| | f``(0) present | f``(0) [1] | -θ`(0) present | -θ`(0) [1] | f``(0) present | f``(0) [1] | -θ`(0) present | -θ`(0) [1] |
| 0.7 | 1.706215 | 1.7063 | 0.764178 | 0.7641 | 0.691957 | 0.6917 | 0.633620 | 0.6332 |
| 7 | 1.517916 | 1.5179 | 1.722378 | 1.7224 | 0.923485 | 0.9235 | 1.546029 | 1.5403 |
| 20 | 1.448489 | 1.4485 | 2.457560 | 2.4576 | 1.003108 | 1.0031 | 2.268245 | 2.2683 |
| 40 | 1.410067 | 1.4101 | 3.100993 | 3.1011 | 1.045935 | 1.0459 | 2.905329 | 2.9054 |
| 60 | 1.390286 | 1.3903 | 3.551205 | 3.5514 | 1.067645 | 1.0677 | 3.352501 | 3.3529 |
| 80 | 1.377407 | 1.3774 | 3.909155 | 3.9095 | 1.081658 | 1.0819 | 3.708557 | 3.7089 |
| 100 | 1.368051 | 1.3680 | 4.211174 | 4.2116 | 1.091777 | 1.0918 | 4.009243 | 4.0097 |

**Table II** Effects of $N_t$, $N_b$ and $N_r$ on $f''(0)$, $-\theta'(0)$ and $-\phi'(0)$ when $A = 0.5,\ \lambda = 1,\ \gamma = 0.5,\ \Delta = 0.5,\ \Pr = 10$ and $Le = 10$.

| $N_b$ | $N_t$ | $N_r$ = 0.5 | | | $N_r$ = 3 | | |
|---|---|---|---|---|---|---|---|
| | | f``(0) | $-\theta'(0)$ | $-\phi'(0)$ | f``(0) | $-\theta'(0)$ | $-\phi'(0)$ |
| 0.1 | 0.1 | 1.86358 | 1.98266 | 2.99959 | 1.29405 | 1.94971 | 2.89209 |
| | 0.3 | 1.87689 | 1.46341 | 3.00885 | 1.20280 | 1.44720 | 2.77490 |
| | 0.5 | 1.89459 | 1.18916 | 3.30288 | 1.17626 | 1.18396 | 2.93645 |
| | 0.7 | 1.91206 | 1.02290 | 3.60614 | 1.17597 | 1.02359 | 3.12943 |
| | 0.9 | 1.92805 | 0.91043 | 3.88186 | 1.18647 | 0.91421 | 3.31690 |
| 0.3 | 0.1 | 1.91563 | 1.10471 | 3.50357 | 1.42727 | 1.09997 | 3.42351 |
| | 0.3 | 1.93714 | 0.89987 | 3.66024 | 1.43308 | 0.89932 | 3.55799 |
| | 0.5 | 1.95564 | 0.78110 | 3.80811 | 1.44766 | 0.78250 | 3.68860 |
| | 0.7 | 1.97137 | 0.70268 | 3.93471 | 1.46449 | 0.70499 | 3.80212 |
| | 0.9 | 1.98482 | 0.64593 | 4.04428 | 1.48123 | 0.64867 | 3.90151 |
| 0.5 | 0.1 | 1.94644 | 0.69021 | 3.53118 | 1.47246 | 0.69207 | 3.45816 |
| | 0.3 | 1.96535 | 0.60599 | 3.66488 | 1.48897 | 0.60871 | 3.58235 |
| | 0.5 | 1.98126 | 0.55157 | 3.77327 | 1.50642 | 0.55460 | 3.68382 |
| | 0.7 | 1.99473 | 0.51253 | 3.86302 | 1.52299 | 0.51563 | 3.76836 |
| | 0.9 | 2.00627 | 0.48247 | 3.93986 | 1.53822 | 0.48556 | 3.84111 |
| 0.7 | 0.1 | 1.96866 | 0.48162 | 3.52373 | 1.50008 | 0.48497 | 3.45396 |
| | 0.3 | 1.98501 | 0.44299 | 3.63003 | 1.51811 | 0.44640 | 3.55514 |
| | 0.5 | 1.99883 | 0.41555 | 3.71507 | 1.53507 | 0.41889 | 3.63650 |
| | 0.7 | 2.01059 | 0.39448 | 3.78574 | 1.55044 | 0.39771 | 3.70439 |
| | 0.9 | 2.02073 | 0.37744 | 3.84655 | 1.56425 | 0.38055 | 3.76297 |
| 0.9 | 0.1 | 1.98555 | 0.36490 | 3.51471 | 1.51965 | 0.36836 | 3.44670 |
| | 0.3 | 1.99995 | 0.34478 | 3.59949 | 1.53721 | 0.34813 | 3.52844 |
| | 0.5 | 2.01221 | 0.32945 | 3.66812 | 1.55312 | 0.33268 | 3.59486 |
| | 0.7 | 2.02272 | 0.31709 | 3.72584 | 1.56730 | 0.32019 | 3.65091 |
| | 0.9 | 2.03182 | 0.30673 | 3.77596 | 1.57994 | 0.30970 | 3.69968 |

**Table III** Effects of $\gamma$ and $\Delta$ on $f''(0)$, $-\theta'(0)$ and $-\phi'(0)$ when $A = 0.5$, $\lambda = 1$, $N_r = 0.5$, $N_t = 0.5$ $N_b = 0.5$, $Pr = 10$ and $Le = 10$.

| $\gamma$ | $\Delta$ | f``(0) | -θ(0) | -ϕ(0) |
|---|---|---|---|---|
| 0. 0 | 0. 0 | 1.74114 | 0.55465 | 3.71225 |
| | 2.0 | 2.42814 | 0.54777 | 3.86815 |
| | 4.0 | 2.94365 | 0.54481 | 3.96362 |
| | 6.0 | 3.37615 | 0.54328 | 4.03332 |
| 2.0 | 0. 0 | 2.27894 | 0.54976 | 3.82839 |
| | 2.0 | 2.82588 | 0.54591 | 3.93648 |
| | 4.0 | 3.27555 | 0.54397 | 4.01254 |
| | 6.0 | 3.66738 | 0.54292 | 4.07146 |
| 4.0 | 0. 0 | 2.69411 | 0.54729 | 3.90496 |
| | 2.0 | 3.16479 | 0.54480 | 3.98909 |
| | 4.0 | 3.56984 | 0.54347 | 4.05272 |
| | 6.0 | 3.93132 | 0.54275 | 4.10394 |
| 6.0 | 0. 0 | 3.05265 | 0.54579 | 3.96396 |
| | 2.0 | 3.47213 | 0.54411 | 4.03302 |
| | 4.0 | 3.84350 | 0.54318 | 4.08770 |
| | 6.0 | 4.18059 | 0.54269 | 4.13297 |